Functional and Clinical Characterization of Variants of Uncertain Significance Identifies a Hotspot for Inactivating Missense Variants in RAD51C

Chunling Hu[1], Anil Belur Nagaraj[1], Hermela Shimelis[1], Gemma Montalban[2], Kun Y. Lee[1], Huaizhi Huang[1], Carolyn A. Lumby[1], Jie Na[1], Lisa R. Susswein[3], Maegan E. Roberts[3], Megan L. Marshall[3], Susan Hiraki[3], Holly LaDuca[4], Elizabeth Chao[4], Amal Yussuf[4], Tina Pesaran[4], Susan L. Neuhausen[5], Christopher A. Haiman[6], Peter Kraft[7], Sara Lindstrom[8], Julie R. Palmer[9], Lauren R. Teras[10], Celine M. Vachon[1], Song Yao[11], Irene Ong[12], Katherine L. Nathanson[13], Jeffrey N. Weitzel[14], Nicholas Boddicker[1], Rohan Gnanaolivu[1], Eric C. Polley[15], Georges Mer[1], Gaofeng Cui[1], Rachid Karam[4], Marcy E. Richardson[4], Susan M. Domchek[13], Siddhartha Yadav[1], Kathleen S. Hruska[3], Jill Dolinsky[4], S. John Weroha[1], Steven N. Hart[1], Jacques Simard[2], Jean Yves Masson[2], Yuan-Ping Pang[1], and Fergus J. Couch[1]

ABSTRACT

Pathogenic protein-truncating variants of *RAD51C*, which plays an integral role in promoting DNA damage repair, increase the risk of breast and ovarian cancer. A large number of *RAD51C* missense variants of uncertain significance (VUS) have been identified, but the effects of the majority of these variants on RAD51C function and cancer predisposition have not been established. Here, analysis of 173 missense variants by a homology-directed repair (HDR) assay in reconstituted *RAD51C*$^{-/-}$ cells identified 30 nonfunctional (deleterious) variants, including 18 in a hotspot within the ATP-binding region. The deleterious variants conferred sensitivity to cisplatin and olaparib and disrupted formation of RAD51C/XRCC3 and RAD51B/RAD51C/RAD51D/XRCC2 complexes. Computational analysis indicated the deleterious variant effects were consistent with structural effects on ATP-binding to RAD51C. A subset of the variants displayed similar effects on RAD51C activity in reconstituted human *RAD51C*-depleted cancer cells. Case–control association studies of deleterious variants in women with breast and ovarian cancer and noncancer controls showed associations with moderate breast cancer risk [OR, 3.92; 95% confidence interval (95% CI), 2.18–7.59] and high ovarian cancer risk (OR, 14.8; 95% CI, 7.71–30.36), similar to protein-truncating variants. This functional data supports the clinical classification of inactivating *RAD51C* missense variants as pathogenic or likely pathogenic, which may improve the clinical management of variant carriers.

Significance: Functional analysis of the impact of a large number of missense variants on RAD51C function provides insight into RAD51C activity and information for classification of the cancer relevance of *RAD51C* variants.

Introduction

The RAD51 recombinase in vertebrate cells assembles as nucleoprotein filaments on single-stranded DNA (1) where it facilitates repair of DNA double-strand breaks (DSB) by homologous recombination (HR) and rescue of stalled and damaged DNA replication forks (2). Five paralogs of RAD51 (RAD51B, RAD51C, RAD51D, XRCC2 and XRCC3), that form RAD51C–XRCC3 and RAD51B–RAD51C–RAD51D–XRCC2 complexes (3–5), have been implicated in maintenance of genome stability through regulation of the core RAD51 recombinase (6–10).

Inherited protein truncating variants in *RAD51C* and *RAD51D* predispose to breast and ovarian cancer (11–15). Pathogenic variants in *RAD51C* (HGNC:9820; NM_058216.3) are associated with high risks (OR>4) of ovarian cancer (16, 17), moderate risk (OR = 2–4) of breast cancer in the general population (11, 12) and among high-risk women (18), and with Fanconi anemia (*FANCO*). Furthermore, family-based segregation studies have suggested that *RAD51C* protein truncating variants (PTV) confer high risks of both breast and ovarian cancer (19). *RAD51C* pathogenic variants have been significantly associated with increased risks of estrogen receptor (ER)-negative and triple-negative breast cancer (TNBC) and serous ovarian cancer (12, 20, 21). In addition, the Breast and Ovarian Analysis of Disease Incidence and Carrier Estimation Algorithm (BOADICEA) model for

[1]Mayo Clinic, Rochester, Minnesota. [2]CHU de Quebec-Université Laval Research Center, Université Laval, Quebec City, Quebec, Canada. [3]GeneDx, Gaithersburg, Maryland. [4]Ambry Genetics, Aliso Viejo, California. [5]Beckman Research Institute of City of Hope, Duarte, California. [6]Keck School of Medicine, University of Southern California, Los Angeles, California. [7]T.H. Chan School of Public Health, Harvard University, Boston, Massachusetts. [8]Department of Epidemiology, University of Washington, Seattle, Washington. [9]Slone Epidemiology Center at Boston University, Boston, Massachusetts. [10]Behavioral and Epidemiology Research Group, American Cancer Society, Atlanta, Georgia. [11]Roswell Park Comprehensive Cancer Center, Buffalo, New York. [12]University of Wisconsin-Madison, Madison, Wisconsin. [13]University of Pennsylvania, Philadelphia, Pennsylvania. [14]Latin American School of Oncology, Sierra Madre, California. [15]University of Chicago, Chicago, Illinois.

C. Hu, A.B. Nagaraj, H. Shimelis, and G. Montalban contributed equally to this article.

Corresponding Author: Fergus J. Couch, Department of Laboratory Medicine and Pathology, Mayo Clinic, Stabile 2-42, 200 First Street SW, Rochester, MN 55905. E-mail: couch.fergus@mayo.edu

Cancer Res 2023;83:2557–71

doi: 10.1158/0008-5472.CAN-22-2319

breast cancer risk prediction was recently extended to incorporate pathogenic variants in RAD51C (22–24) and a similar epithelial ovarian cancer (EOC) model for ovarian cancer risk prediction incorporating variants in RAD51C was developed (25).

Testing of *RAD51C* for germline pathogenic variants using clinical hereditary cancer panels has identified more than 750 variants of uncertain significance (VUS; https://clinvarminer.genetics.utah.edu), composed predominantly of missense and intronic variants. These VUS pose an ongoing challenge for clinical management of VUS carriers. Currently, there is no established method for systematic clinical evaluation of the contribution of *RAD51C* VUS to cancer risk because FDA approved ClinGen rules for classification of *RAD51C* variants based on ACMG/AMP models (26) are not yet available. However, functional studies provide insight into the influence of *RAD51C* VUS on protein function, cancer risk, and response to therapy. To date, only a small number of missense variants have been assessed for effects on RAD51C function (7, 8, 27). To better understand the cancer relevance of *RAD51C* variants, we present a comprehensive analysis of the influence of 173 missense VUS on HR repair, response to cisplatin and PARP inhibition, RAD51C protein conformation, and risk of breast and ovarian cancers.

Materials and Methods

RAD51C missense VUS selection

RAD51C missense variants were selected from several sources. A total of 34 were identified in public databases (ClinVar, gnomAD, EXAC, COSMIC, LOVD). All 34 *RAD51C* missense variants observed in 6,667 Caucasian ovarian cancer cases tested at Ambry Genetics from March 2015 to December 2017, all 94 high-quality (PASS) *RAD51C* missense variants observed in non-Finnish European (NFE) gnomAD exome public reference controls by December 2017, and 11 *RAD51C* variants previously evaluated for functional effects in other studies were included in the study, for a total of 173 *RAD51C* missense variants (Supplementary Table S1). All variants were evaluated for effects on splicing using the Splice AI algorithm (Supplementary Table S1). The p.Ser16Gly (S16G), p.Asp108Gly (D108G), p.Cys135Tyr (C135Y), p.Lys235Asn (K235N), and p.Leu262Val (L262V) variants were predicted to cause aberrant splicing (Splice AI score>0.5) and were excluded from case–control association studies.

Homology-directed repair reporter assay

Each *RAD51C* variant was introduced into a mammalian h*RAD51C* expression construct using site-directed mutagenesis. CL-V4B *RAD51C*-deficient Chinese hamster cells, previously used for RAD51C functional studies (8, 28, 29), stably expressing the DR-GFP reporter construct (provided by Dr. Ralph Scully, Beth Israel Deaconess Medical Center and Harvard Medical School, Boston, MA) were used for homology-directed repair (HDR) assays. DR-GFP CL-V4B cells were co-transfected with either wild-type (WT) or mutant *RAD51C* plasmids and pCBASce1 plasmid expressing iSce1 using X-tremeGENE 9 DNA transfection reagent (Roche). After 72 hours, cells expressing GFP were quantified by FACS analysis. The numbers of GFP-positive cells were normalized and rescaled to a 1:5 ratio derived from the p.Leu138Phe (L138F) consensus pathogenic variant control reported in ClinVar and the neutral WT *RAD51C* control (30). The p.Ala126Thr (A126T) variant served as a positive control in addition to the WT protein based on a frequency of 0.006 for the general population in dbSNP. All variants were analyzed in duplicate in at least two independent experiments. RAD51C expression was assessed by Western blotting with anti-RAD51C mouse mAb (mAb F11; Santa Cruz Biotechnology) and anti-FLAG mouse monoclonal (mAB M2; Sigma; ref. 6).

Drug response assay

RAD51C missense variants were introduced into the pLentiGFP vector harboring a WT *RAD51C* cDNA using site-directed mutagenesis. Lentivirus was produced in 293T cells using ViraPower packaging mix (Thermo Fisher Scientific) following transfection by Lipofectamine 3000 (Thermo Fisher Scientific). CL-V4B cells were transduced with lentivirus expressing either WT or mutant *RAD51C*. Expression of *RAD51C* was confirmed by immunofluorescence and Western blot analysis. After 24 hours, 1,000 cells per well were exposed to various doses of cisplatin or olaparib for 16 hours, grown for 5 days after drug treatment, and subjected to an MTS colorimetric assay (CellTiter 96 AQueous One Solution Cell Proliferation Assay; Promega). WT and the consensus pathogenic C135Y variant reported in ClinVar were used as controls. Cell proliferation relative to untreated control was determined for all variants. IC_{50} values were determined using a nonlinear regression dose–response variable slope equation in GraphPad Prism 7. IC_{50}s were normalized to a 1:15 ratio derived from the C135Y and WT control. All variants were analyzed in six technical replicates in at least two independent experiments.

RAD51C foci indirect immunofluorescence assay

CL-V4B cells transduced with WT or *RAD51C* missense variant lentivirus were irradiated with γ-IR (5 Gy) and after 6 hours were fixed with 2% paraformaldehyde. Cells were incubated with primary antibodies [RAD51C (IgG1 mouse monoclonal, Santa Cruz Biotechnology), geminin (IgG2b mouse monoclonal, Santa Cruz Biotechnology) and RAD51 (rabbit polyclonal, Abcam)]. Cells were subsequently incubated with secondary antibodies [anti-mouse IgG1 AF488, anti-mouse IgG2b AF647 and anti-rabbit AF568 (Thermo Fisher Scientific)] for 1 hour. Z stack images were acquired using an inverted Zeiss LSM 780 confocal microscope system. Geminin-high cells (n = 1,000) positive and negative for RAD51 foci were counted and the mean percentage of geminin-high cells positive for RAD51 foci was plotted (Supplementary Fig. S1). All variants were analyzed in three independent experiments.

Characterization of *RAD51C*$^{-/-}$ landing pad cell lines reconstituted with *RAD51C* variants

The landing pad genomic locus was integrated into U2OS *RAD51C*$^{-/-}$ cells [Leibniz Institute (U2OS#18-RAD51C-15; DSMZ ACC 834)] as previously described (31). Briefly, cells were transduced with a lentivirus containing a Bxb1 recombination site (pLenti-TetBxb1BFP-2A-iCasp9–2A-Blast_rtTA3) and selected with blasticidin (1 μg/mL) for two weeks. *RAD51C* missense variants were introduced into the VAMPseq plasmid (attB-FLAG-RAD51C-IRES-mCherry-562bgl-KanR) containing *RAD51C* sequence by site-directed mutagenesis. Cells were cotransfected with the Bxb1 recombinase (CAG-Bxb1) and the *RAD51C* constructs [WT, L138F, p.Gly130Arg (G130R), p.Lys131Ile (K131I), p.Thr132Arg (T132R), p.Gln133Glu (Q133E), p.Arg168Gly (R168G) and p.Gly302Val (G302V); selected on the basis of deleterious activity in the HDR assay and predicted interaction with ATP in the conformational model] using X-tremeGENE 9 Transfection Reagent (Roche; Supplementary Fig. S2). Recombined U2OS *RAD51C*$^{-/-}$ landing pad cells were selected with AP1903 (10 nmol/L) for 48 hours and RAD51C expression was induced with doxycycline (2 μg/mL). mCherry-positive cells were enriched by cell sorting (BD FACSAria Fusion cytometer) and expanded with blasticidin and doxycycline for 2–3 weeks. RAD51C

expression was assessed by Western blotting with mouse mAb (mAb 2H11; Santa Cruz Biotechnology; ref. 6) after 24 hours of doxycycline induction. mCherry expression was also confirmed by microscopy in a Cytation 5 Cell Imaging Multi-Mode Reader.

Drug sensitivity analysis of landing pad cells

U2OS *RAD51C*$^{-/-}$ landing pad cells carrying *RAD51C* variants were seeded at a density of 3,000 cells per well. Doxycycline and blasticidin were removed from the media at the time of plating. After 24 hours, cells were treated at increasing concentrations of olaparib for 4 days. Nuclei were stained with Hoechst 33342 (Invitrogen) and quantified by image acquisition using a Cytation 5 Cell Imaging Multi-Mode Reader (32). The percentage of surviving cells was calculated relative to mock-treated cells. Experiments were performed in triplicate unless denoted otherwise.

Quantification of RAD51 foci in landing pad cells

Stable landing pad U2OS cells expressing *RAD51C* variants were irradiated with 5 Gy (CellRad, Precision X-Ray) and fixed with 4% paraformaldehyde 4 hours postirradiation. Cells were incubated for 1 hour with anti-RAD51 (polyclonal; Bioacademia #70–001) and anti-geminin (monoclonal; Abcam #ab104306) antibodies (32), and secondary antibodies [Alexa Fluor 488 goat anti-rabbit (Thermo Fisher Scientific, #A-11008) and Alexa Fluor 647 goat anti-mouse (Thermo Fisher Scientific #A-21235)] and stained with DAPI. Z-stack microscopy images from a 50x water immersion objective were automatically acquired for 1,000 geminin-positive (S/G_2 phase) cells per variant in a Cell discoverer 7 instrument (Zeiss). Images were processed and analyzed using ZEN (blue edition) Celldiscoverer 3.2 (Zeiss) software. Each *RAD51C* variant was assessed in triplicate, unless denoted otherwise.

Colony formation assays

Each landing pad cell line was plated in a 6-well plate at a density of 1,000 cells/well and cultured for two weeks. Media containing blasticidin and doxycycline were refreshed every three days. After two weeks, cells were washed with PBS, fixed, and stained with 0.5% crystal violet solution for 30 minutes to 1 hour. Each variant was assessed in three independent experiments performed in duplicate. Clonogenic assays were quantified manually using ImageJ software.

RAD51C immunoprecipitation with RAD51 paralogs

HEK293T cells and CL-V4B cells were transfected with Flag-tagged *RAD51C* WT and variant expression plasmids. After 48 hours, cells were lysed with 50 mmol/L Tris HCl pH 7.5, 300 mmol/L NaCl, 5 mmol/L EDTA pH 8, 0.5% NP-40. Lysates were incubated with anti-Flag M2 (Sigma) antibody and protein G agarose beads (Roche) for immunoprecipitation. Proteins were resolved on 4%–15% gradient Tris-HCl gels (Bio-Rad), transferred to polyvinylidene difluoride membrane (Millipore), and incubated with XRCC3, XRCC2, RAD51D, and RAD51C (Santa Cruz Biotechnology) polyclonal antibodies.

Cell culture

All cells were grown in DMEM supplemented with 10% FBS and 1% penicillin/streptomycin. All cell lines were authenticated by sequencing of mutated regions and/or by genotype fingerprinting using polymorphism panels.

In silico prediction

Missense prediction scores from three predictors (REVEL, VEST4, and M-CAP) were obtained from dbSNFP v4.0 for 173 RAD51C missense mutations (33). RankScores that were associated with transcript ENST00000337432 and gene ID ENSG00000108384 were chosen. Receiver operating characteristic curve (ROC), optimized thresholds, and sensitivity and specificity were calculated using pROC (version 1.15), ROCR (version 1.0.7), and caTools (version 1.17.1.2).

Structural models

A homology model of monomeric apo RAD51C was developed using the SWISS-MODEL server (34) based on the cryogenic electron microscopy structure of RAD51 (Protein Data Bank ID: 5NP7; ref. 35). A model of an apo RAD51C dimer was also derived from 5NP7 using SWISS-MODEL and refined with 20 31.6-ns MD simulations using FF12MC, a protein forcefield (36). This set of simulations showed that the dimer was relatively stable except for residues 1–83 and 176–200 in each monomer that comprise four intrinsically unstable surface regions. An ATP-bound RAD51C dimer was developed by manually inserting ATP into the dimer interface of the MD-refined apo RAD51C dimer using PyMOL V1.7.0.3 (https://pymol.org) guided by the 5NP7 structure in which an ATP analogue binds at the protein–protein interface. The ATP-bound RAD51C dimer was refined by 20 316-ns MD simulations after truncation of the four intrinsically unstable surface regions using FF12MC. This was followed by 100 63.2-ns MD simulations of the ATP-bound full-length RAD51C dimer with the core domain adopting the most populated conformation in the 20 316-ns MD simulations. The most populated conformation of the ATP-bound full-length RAD51C dimer in the 100 63.2-ns MD simulations was used as the theoretical (three-dimensional, 3D) model for evaluation of missense variants in *RAD51C* (Supplementary Data).

Clinical assessment

The study was approved by the Mayo Clinic institutional review board. The GeneDx and Ambry Genetics studies were conducted in accordance with guidelines set forth by the Western Institutional Review Board (WIRB). WIRB waived authorization for use of deidentified aggregate data for cases and controls for GeneDx. The Ambry Genetics study of the clinical-testing cohort was deemed exempt from review by the WIRB. Written informed consent for genetic testing was obtained from all individuals. The study included all patients with ovarian and breast cancer receiving hereditary cancer clinical genetic testing with gene panels including *RAD51C*, prior to 4/2020, by Ambry Genetics and GeneDx. Controls were noncancer, female reference controls from gnomAD and the population-based CARRIERS study. Counts of individual missense variants classified as deleterious by the HDR assay among breast and ovarian cancer cases subjected to hereditary cancer testing were pooled and compared with pooled counts of HDR defined deleterious variants from gnomAD2.1 and gnomAD3.1 noncancer, female reference controls and population-based noncancer, female controls from the CARRIERS breast cancer case–control study (12). Similar comparisons were performed for HDR-defined neutral variants and PTVs.

Statistical analysis

Breast and ovarian cancer case–control association analyses were performed using a weighted logistic regression with control populations weighted for the relative frequency of different races and ethnicities in cases. Analyses restricted to non-Finnish Europeans and non-Hispanic whites were performed using Fisher exact test. OR>2 was considered moderate risk and OR>5 was considered high risk.

Data availability

The functional data generated in this study are available within the article and supplementary data files and are also available upon request

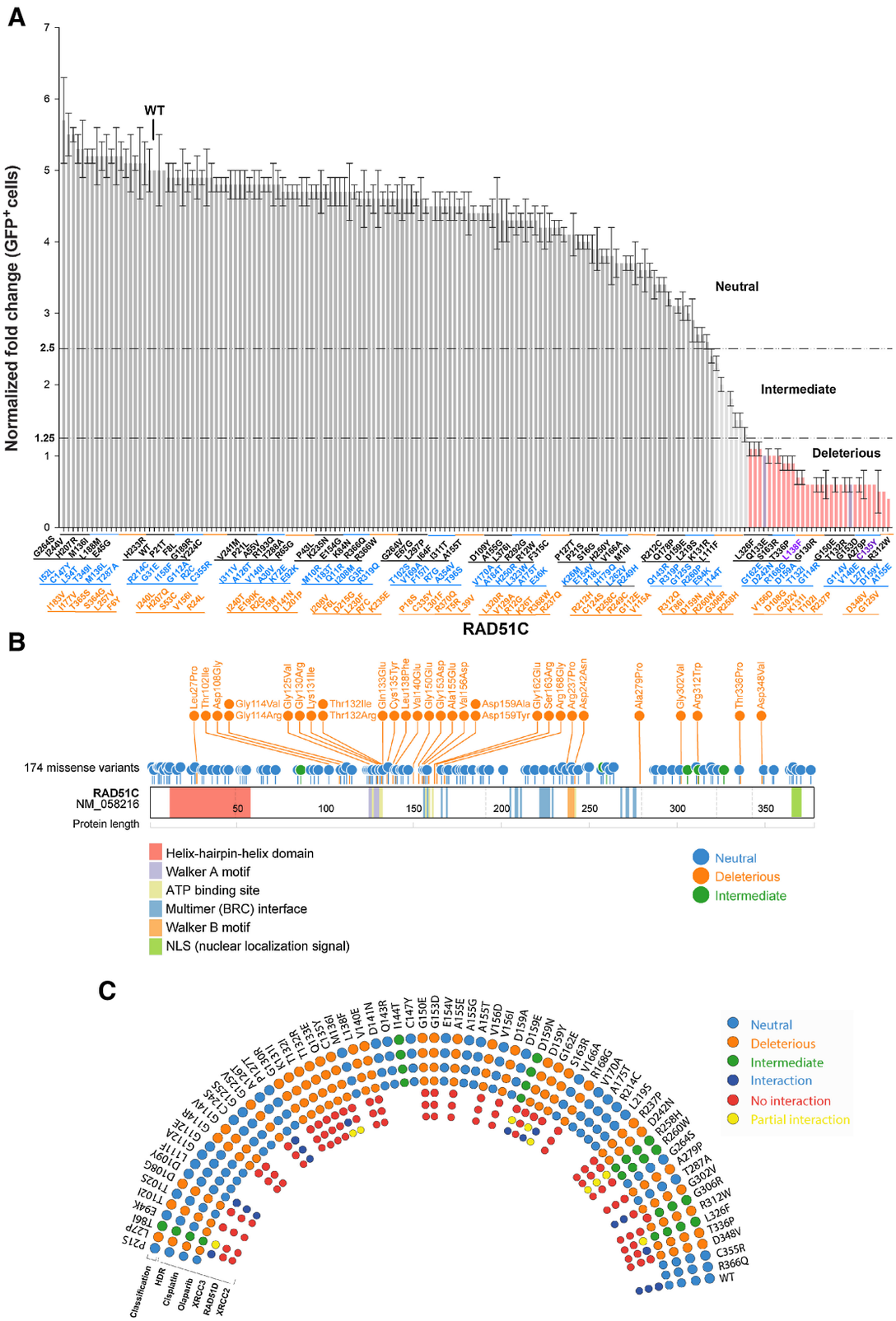
A
Normalized fold change (GFP+ cells)
WT
Neutral
Intermediate
Deleterious
RAD51C
B
174 missense variants
RAD51C
NM_058216
Protein length
Helix-hairpin-helix domain
Walker A motif
ATP binding site
Multimer (BRC) interface
Walker B motif
NLS (nuclear localization signal)
Neutral
Deleterious
Intermediate
C
Neutral
Deleterious
Intermediate
Interaction
No interaction
Partial interaction
Classification
HDR
Cisplatin
Olaparib
XRCC3
RAD51D
XRCC2

from the corresponding author. The cryoEM data analyzed in this study were obtained from Protein Data Bank ID: 5NP7 (https://www.rcsb.org/structure/5np7). The Rad51 variants were extracted from ClinVar (https://www.ncbi.nlm.nih.gov/clinvar/) and gnomAD (https://gnomad.broadinstitute.org/). Data for case–control association studies were obtained from gnomAD (https://gnomad.broadinstitute.org/) and the CARRIERS study (dbGAP phs002820.v1.p1).

Results

Functional assessment of the 173 *RAD51C* missense variants with HDR assay

A cell-based DR-GFP HDR colorimetric reporter assay was used to assess the influence of 173 missense mutations on RAD51C HR DNA repair activity (Supplementary Table S1). *RAD51C* deficient CL-V4B cells (28) were reconstituted with full-length *RAD51C* expression constructs and HDR levels were quantified relative to WT and the known deleterious L138F mutant. Of these, 30 variants had reduced RAD51C HDR activity (normalized HDR scores <1.25; estimated as <25% activity) and were categorized as deleterious; 8 variants exhibited partial HDR activity (normalized HDR scores <2.5, >1.25; estimated as 25–50% activity) and were categorized as hypomorphic; and 135 variants retained high levels of activity (normalized HDR score >2.5; estimated as >50% activity) and were categorized as neutral (**Fig. 1A**; Supplementary Table S1). These activity thresholds were consistent with results from *BRCA2* and *PALB2* functional assays (37, 38). A hotspot (residues 125–168), containing the Walker A phosphate binding P-loop of RAD51C that contributes to ATP-binding, included 18 of the 30 deleterious variants (**Fig. 1B**). Other deleterious variants were spread across the protein with two in the ATP-binding Walker B motif. Among missense variants evaluated in other studies, 5 of 7 deleterious variants (C135Y, p.Gly125Val (G125V), p.Gly153Asp (G153D), p.Arg312Trp (R312W), and L138F) were deleterious in the HDR assay and two ((p.Gln143Arg (Q143R), p.Leu219Ser (L219S)) were neutral (Supplementary Table S1). Of six previously reported intermediate variants, four were neutral [p.Arg214Cys (R214C), p.Gly264Ser (G264S), p.Thr287Ala (T287A), and p.Arg366Gln (R366Q)] and two [p.Asp159Asn (D159N) and p.Arg258His (R258H)] were intermediate in the HDR assay. All four reported neutral variants [p.Gly3Arg (G3R), A126T, p.Val169Ala (V169A), and p.Gly264Val (G264V)] remained neutral in the HDR assay. The WT and mutant forms of RAD51C expressed equally (Supplementary Table S1).

Influence of *RAD51C* missense mutation on response to cisplatin and olaparib

RAD51C loss promotes HR deficiency and sensitizes cells to cisplatin and olaparib PARP inhibitor (39–41). Thus, the influence of 60 *RAD51C* missense variants from the HDR assay (30 deleterious, 23 neutral, and 7 intermediate) on cisplatin and olaparib response in CL-V4B cells was evaluated. Most deleterious variants (26 of 30) displayed IC_{50} values that were <25% of WT (**Figs. 1C**, **2A** and **B**; Supplementary Tables S1 and S2), consistent with HDR assay results (**Fig. 1A**). The remaining 4 deleterious variants exhibited IC_{50}s of 30%–40% WT. IC_{50} values for neutral variants ranged from 84% to 111% WT for both drugs (Supplementary Table S2), except for p.Glu94Lys (E94K) (97% for cisplatin and 54% for olaparib). IC_{50} values for 6 of the 7 intermediate variants ranged from 40% to 80% WT for both drugs. However, p.Gly306Arg (G306R) exhibited 51% IC_{50} for cisplatin and 27% IC_{50} for olaparib and was 31% of WT in the HDR assay, suggesting a partial/hypomorphic effect.

Impact of *RAD51C* missense variants on RAD51 foci formation

An inability to form RAD51 foci at the sites of DNA DSBs is a key component of an HR deficient phenotype. Because disruption of RAD51C substantially decreases RAD51 foci formation (8, 42) the influence of *RAD51C* missense variants on RAD51 foci formation in CL-V4B cells in response to irradiation-induced DNA damage was evaluated. WT *RAD51C* and neutral variants [p.Pro21Ser (P21S), p.Asp109Tyr (D109Y) and p.Cys147Tyr (C147Y)] induced RAD51 foci formation, whereas the deleterious variants [p.Asp108Gly (D108G), C135Y, p.Val140Glu (V140E), p.Ala155Glu (A155E) and p.Asp159Tyr (D159Y)] exhibited dramatically reduced RAD51 foci formation and the p.Gly306Arg (G306R) intermediate variant exhibited partially reduced foci (Supplementary Fig. S1). The results were fully consistent with the HDR assay and drug response findings.

Functional effects of *RAD51C* variants in human cells

To confirm the functional effects of *RAD51C* variants in a human cell line, *RAD51C* WT and 7 deleterious or intermediate missense variants in the HDR assay (G130R, K131I, T132R, Q133E, L138F, R168G and G302V) were introduced into a U2OS *RAD51C*$^{-/-}$ cell line containing a landing pad site, which allowed for stable expression of variants (Supplementary Fig. S2). The G130R, K131I, T132R, and R168G HDR deleterious variants showed sensitivity to olaparib compared with WT-complemented cells, whereas the Q133E and G302V variants had intermediate effects (**Fig. 3A**). Some variability in expression of some mutant proteins was observed in the U2OS *RAD51C*$^{-/-}$ landing pad cells (**Fig. 3B**). However, no differences in 3- and 6-hour protein half-life of the landing pad variants displaying variation in expression were observed following cycloheximide treatment of 293T cells (Supplementary Table S1).

In parallel, a recent study evaluated the influence of 36 RAD51C missense variants on HR activity of U2OS and 21 on HR activity of MCF10A cells (27). Importantly, 18 of 36 evaluated in U2OS and 13 of 21 evaluated in MCF10A cells were also characterized in this study (Supplementary Table S1). All 8 variants with reduced activity in U2OS cells (HDR score < 0.5), which approximates to 50% activity,

Figure 1.

Evaluation of 173 *RAD51C* missense variants by HDR assay. **A,** DR-GFP reporter assay showing the range of HDR activity for 173 missense variants in CL-V4B cells, measured as fold change in GFP-positive cells (normalized to 1–5 scale, WT = 5 and p.Leu138Phe = 1). Neutral (>2.5 scale, gray bars), deleterious (<1.25 scale, red bars), and intermediate effects (>1.25, <2.5 scale, light gray bars). Purple, L138F and C135Y deleterious controls. Amino acid changes in one letter code are labeled on the *x*-axis in clusters (black, blue, and orange) in order of presentation on the bar chart. Error bars, SEM of three independent experiments. **B,** Illustration of the location of missense variants within the RAD51C linear sequence identifying a deleterious variant hotspot. Key functional domains of RAD51C are indicated and neutral (blue), deleterious (orange), and intermediate (green) variants are shown at top. **C,** Circos plot of the RAD51C variants and functional assay (HDR, cisplatin and olaparib sensitivity, binding to XRCC3, RAD51D, and XRCC2) results. RAD51C variants are indicated by residue position in the outer ring. Track 1 shows the final score based on all functional assays. For HDR, variants were classified as neutral (light blue; ≥51.1% relative to WT), intermediate (green; 48.7%–26.8%), or deleterious (orange; ≤22.7%). Cisplatin sensitivity was classified as neutral (≥83.5% relative to WT), intermediate (43%–82%), or deleterious (≤13.1%). Olaparib sensitivity was classified as neutral (≥ 80.4% relative to WT), intermediate (78.7%–51.7%), or deleterious (≤42%). Dark blue, interactions with XRCC3, RAD51D, and XRCC2; yellow, partial interaction; red, no interaction.

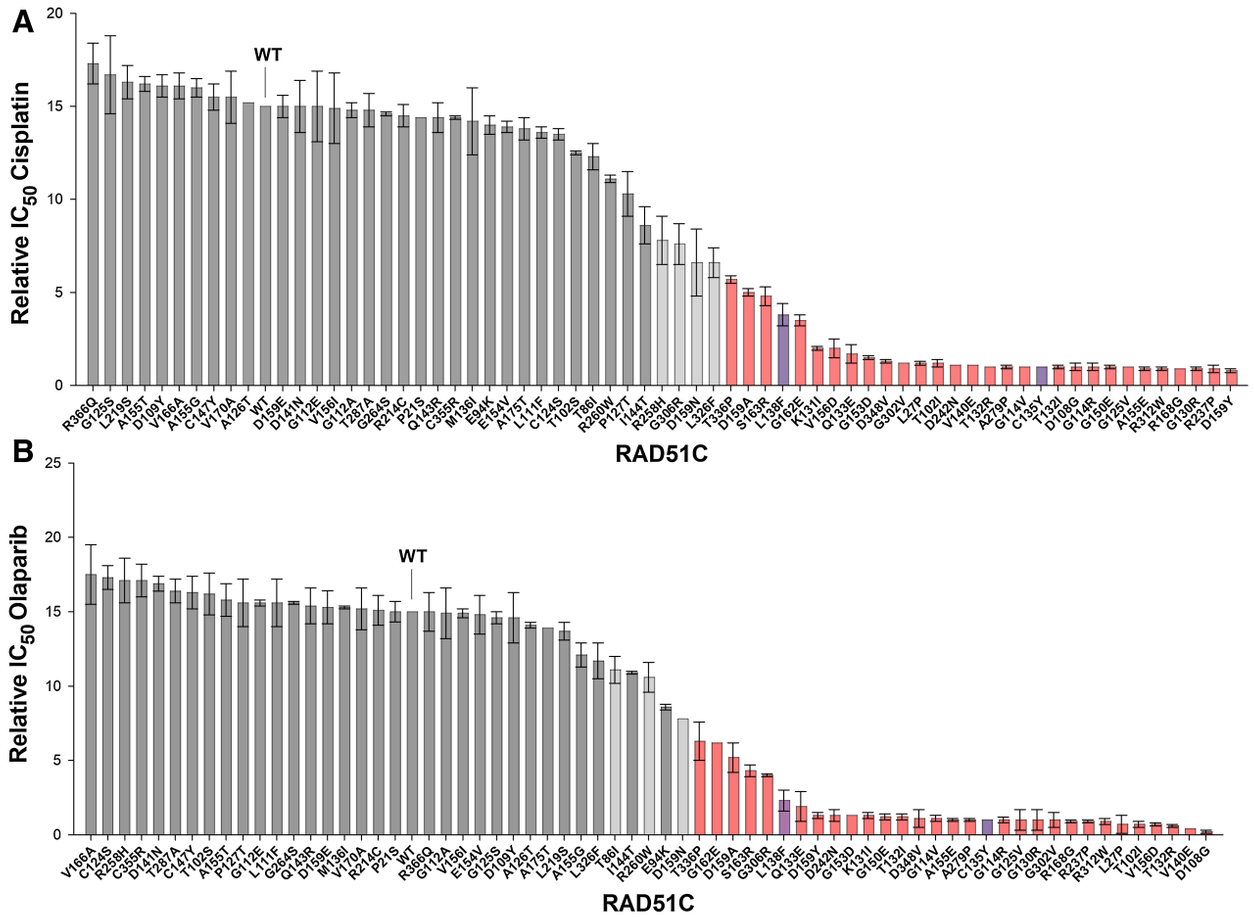

Figure 2.

Influence of RAD51C missense variants on response to cisplatin and olaparib treatment. Relative IC_{50} values (normalized to 1–15 scale, WT = 15 and p.Cys135Tyr = 1) from an MTS assay of CL-V4B cells, transduced with selected RAD51C variant lentivirus, 5 days after treatment with varying doses of cisplatin (**A**) and olaparib (**B**). Variants defined as neutral (gray), intermediate (light gray), and deleterious (red) by the HDR assay are shown. Purple, L138F and C135Y deleterious controls. Error bars, SEM of three independent experiments.

had CL-V4B HDR scores < 1.5 (approximates to 30% activity) in the current study. Similarly, all 6 variants with HDR scores <0.5 in MCF10A cells had CL-V4B HDR scores < 1.5 (Supplementary Table S1). Interestingly the established deleterious L138F variant, which was used as a negative control (HDR score = 1.0) in the CL-V4B studies, also showed low activity in U2OS cells (HDR score = 0.19), but had WT levels of activity (HDR score = 0.94) in MCF10A cells (Supplementary Table S1; ref. 27). Similarly, several other variants showed higher activity in MCF10A cells compared with results in U2OS cells and the results from the current CL-V4B studies (Supplementary Table S1), suggesting that the published MCF10A cell studies may need further calibration. Overall, however, the consistency between HDR assays conducted in CL-V4B cells and human MCF10A breast and U2OS osteosarcoma cells suggests that the results in CL-V4B cells reflect effects in human breast cancer cells. Interestingly, comparisons of cisplatin and olaparib response assays in CL-V4B cells with the HDR results from U2OS and MCF10A also showed consistency. All 8 variants with HDR scores <0.5 in U2OS cells showed sensitivity to cisplatin and 7 of 8 showed sensitivity to olaparib in CL-V4B cells. Likewise, all 6 variants with HDR scores <0.5 in MCF10A cells showed sensitivity to cisplatin and 5 of 6 showed sensitivity to olaparib in CL-V4B cells. Thus, HDR and two different drug sensitivity assays show consistency with MCF10A and U2OS HDR results.

Because RAD51C participates in DNA damage signaling by regulating cell cycle progression (43), colony formation assays were performed to evaluate the influence of *RAD51C* variants on cell proliferation. U2OS *RAD51C*$^{-/-}$ landing pad cells complemented with G130R, K131I, T132R, L138F, and R168G variants showed a proliferation defect, whereas Q133E and G302V cells displayed a WT phenotype (**Fig. 4A**). Formation of RAD51 foci in response to ionizing radiation was also assessed by automated microscopy (**Fig. 4B**). A decrease in RAD51 foci was observed for parental and L138F reconstituted cells (91% and 78% mean changes, respectively) relative to WT-complemented cells. Cells expressing G130R, K131I, T132R, and R168G variants showed a significant decrease in RAD51 foci, with mean changes ranging from 73% to 96%, whereas the Q133E and G302V variants yielded an intermediate phenotype. Overall, *RAD51C* variants that disrupted HR repair in CL-V4B cells had very similar effects in human U2OS cells.

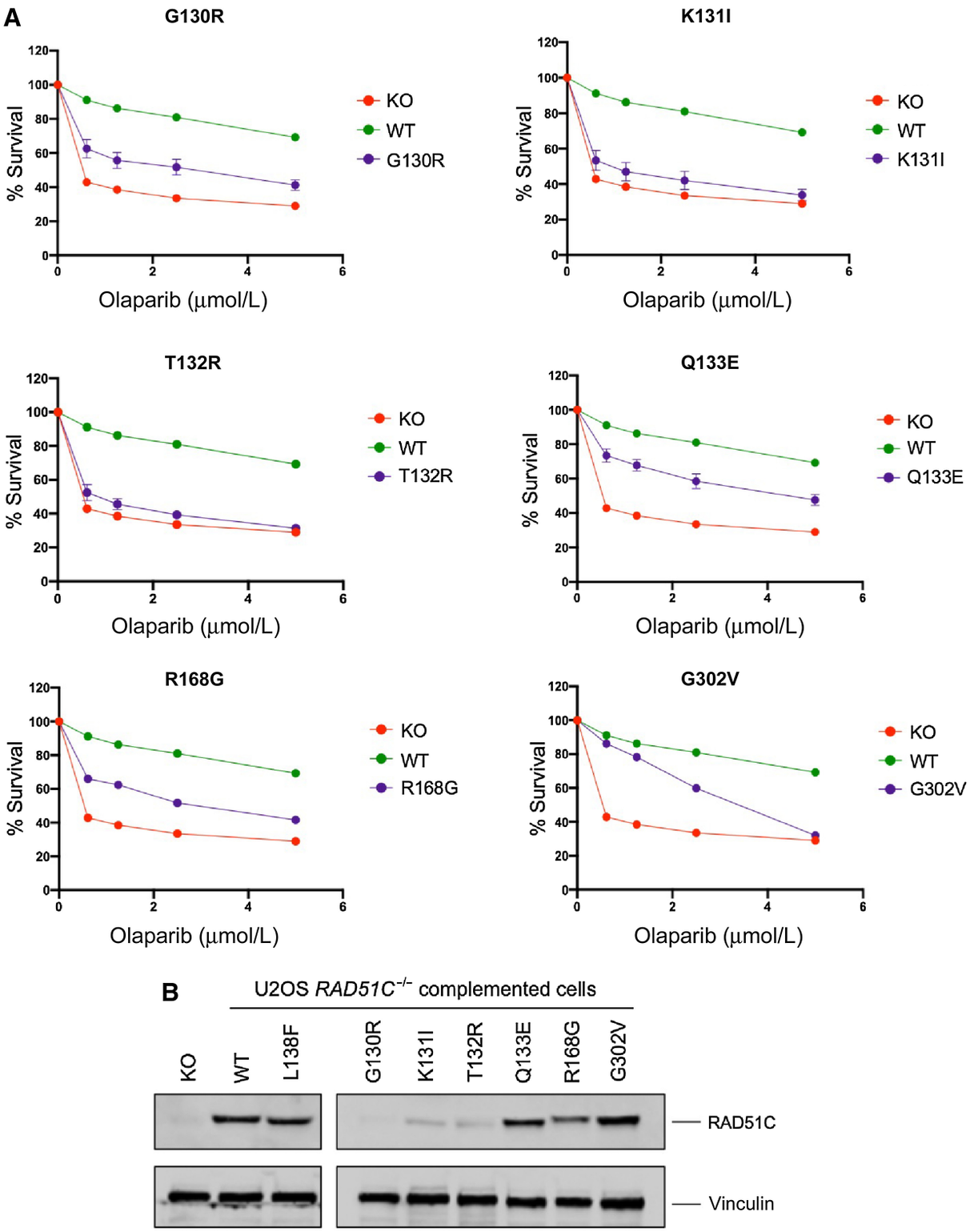

Figure 3.

Drug sensitivity of human U2OS landing pad cells. **A,** Olaparib sensitivity associated with *RAD51C* variants. Cell survival of U2OS cells expressing RAD51C variants was quantified after 4 days of treatment and calculated relative to mock-treated cells. Mean ± SEM was calculated from three independent experiments, each performed in triplicate. **B,** RAD51C protein levels in stable U2OS landing pad cell lines. Expression of RAD51C WT and variant proteins in U2OS cells was determined by Western blot analysis after 24 hours of doxycycline induction.

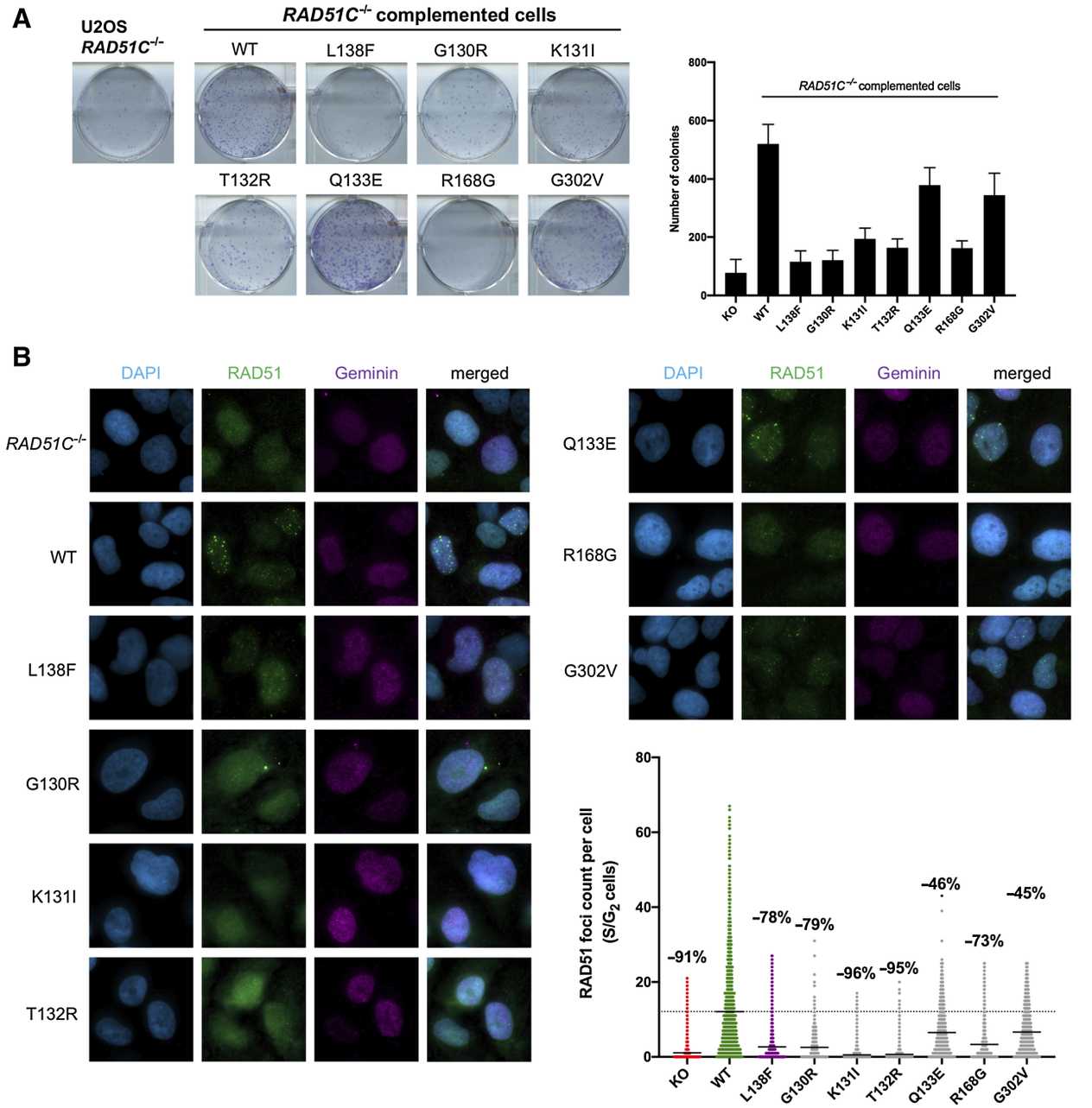

Figure 4.

Characterization of U2OS landing pad cells expressing RAD51C variants. **A,** Colony formation assays of *RAD51C* variants. **B,** RAD51 foci quantification and representative microscopy images for each variant. RAD51 foci formation was quantified after exposure of landing pad cells to 5 Gy of γ-irradiation. Each dot represents a geminin (S/G_2 phase)-positive cell and the bars designate the mean number of foci in at least 1,000 cells obtained in at least three independent experiments. The mean change percentage was calculated for each variant relative to the WT.

Intrinsic RAD51C protein complex formation

RAD51C forms the BCDX2 and CX3 complexes that are involved in RAD51 recruitment to sites of DNA damage (39). To evaluate the influence of RAD51C variants on the integrity of these intrinsic complexes, coimmunoprecipitation of ectopically expressed FLAG-tagged RAD51C WT and variant proteins with endogenous RAD51D, XRCC2, and XRCC3 in HEK293T cells was performed. WT RAD51C and the known neutral variants, A126T and D109Y, coimmunoprecipitated with XRCC3 (CX3 complex) and with both RAD51D and XRCC2 (BCDX2 complex; **Fig. 5**). In contrast, the L138F known deleterious variant did not coimmunoprecipitate with these proteins (**Fig. 5**). All 30 HDR deleterious variants from the HDR assay lost the ability to form at least one of the CX3 and BCDX2 complexes (**Fig. 5**; Supplementary Table S3), whereas none of the neutral variants

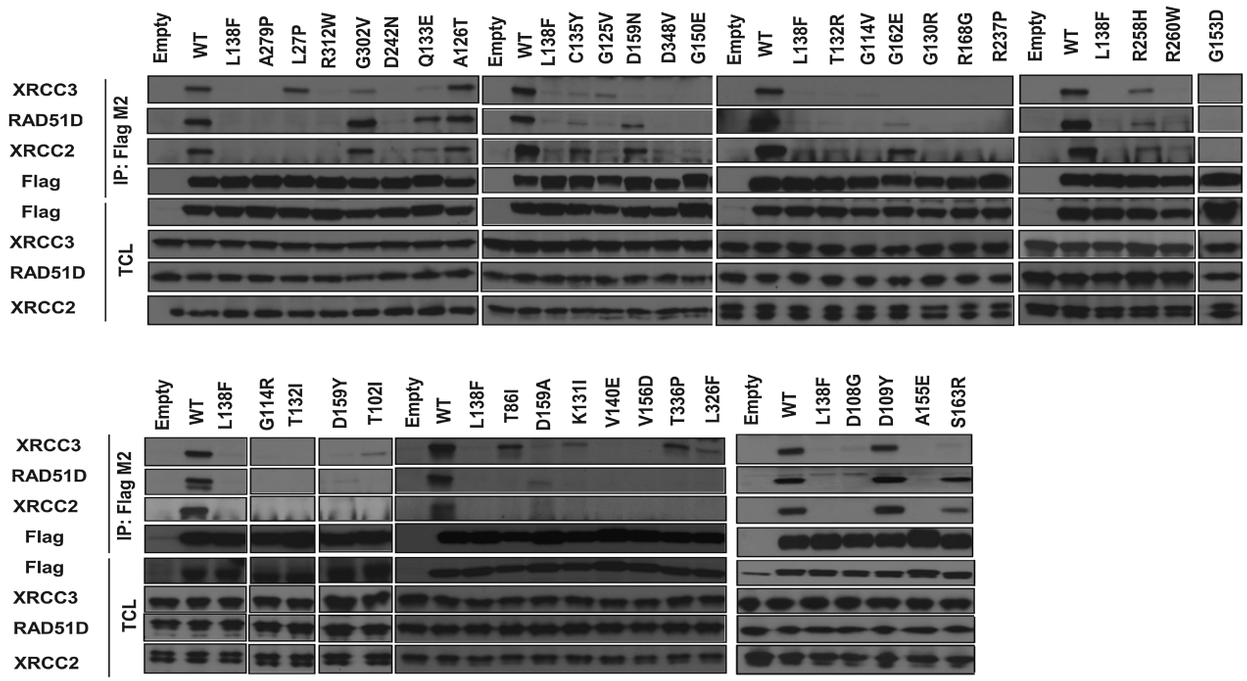

Figure 5.

Coimmunoprecipitation analysis of RAD51C CX3 and BCDX2 complexes. Western blotting of coimmunoprecipitated Flag-tagged RAD51C variant proteins with XRCC3 and RAD51D, XRCC2 paralogs 48 hours after transfection of HEK293T cells with FLAG-tagged RAD51C variant expression plasmids. IP, immunoprecipitation; TCL, total cell lysate.

interfered with intrinsic complex formation (Supplementary Table S3). The p.Leu27Pro (L27P) and p.Thr336Pro (T336P) deleterious variants and the p.Thr86Ile (T86I) intermediate variant bound only to XRCC3 and not to RAD51D-XRCC2. In addition, the Q133E, p.Gly162Glu (G162E), p.Ser163Arg (S163R), and G302V HDR deleterious variants and the D159N intermediate variant lost the ability to bind to XRCC3 but were able to bind to RAD51D-XRCC2. Furthermore, the R258H variant, observed as a homozygous variant in a FANCO patient, displayed reduced binding for all complex members (**Fig. 5**; Supplementary Table S3).

Computational analysis of variant effects on ATP binding to RAD51C

Structural details can provide mechanistic insight into variant effects on protein function. However, the structure of the RAD51C protein had not been experimentally determined at the time of this study. Initially, a homology model of apo-RAD51C monomer was developed using SWISS-MODEL (Supplementary Fig. S3; ref. 34), but this model lacked a RAD51C ATP-binding site (44). Importantly, while RAD51C can form ATP-associated BCDX2 and CX3 paralog complexes and the *Saccharomyces cerevisiae* RAD51 paralog complex (RAD55–RAD57) promotes assembly of RAD51 filaments through transient ATP-associated oligomeric interactions (45), gel filtration studies have suggested that RAD51C can also form a homotetramer (44), and SWISS-MODEL analysis based on the cryoEM structure of RAD51 (35) for this study suggested existence of a RAD51C oligomer, with ATP binding at the protein–protein interfaces. Thus, a theoretical model of a RAD51C dimer with ATP bound at the dimer interface—as the minimal representation of RAD51C protomers—was developed, tested, and refined with molecular dynamics simulations using the FF12MC protein forcefield (**Fig. 6**; Supplementary Fig. S4; ref. 36). Simulations with an aggregated 12.64 microsecond simulation time yielded a stable dimer with an ATP-binding site that shielded the ATP from solvent and enabled formation of salt bridges of the ATP phosphate groups with K131 and R168 from one RAD51C monomer and R312 and K328 from the other. This model revealed the locations of the 60 missense RAD51C VUS relative to the ATP-binding site. Most variants were located in the well-structured core domain, except for the P21S, T86I, and E94K HDR neutral variants, located in the flexible *N*-terminal domain (**Fig. 6A**). Importantly, 8 of 12 missense variants from the core 130–140 helical region that abuts the ATP molecule were predicted to disrupt the ATP-binding site, and all 8 were subsequently shown to be deleterious in the HDR assay (**Fig. 6**; Supplementary Table S4). K131I and R168G remove positively charged residues that directly interact with the negatively charged triphosphate group of ATP; Q133E introduces a negatively charge group that destabilizes the negatively charged triphosphate group; G130R, p.Thr132Ile (T132I), T132R, p.Cys135Tyr (C135Y), L138F, and p.Val140Glu (V140E) introduce a charged or bulky group into a tight hydrophobic pocket that may destabilize the residue 130–140 helical region. While these 9 HDR deleterious variants influence RAD51C function due to positions in the first monomer, 2 deleterious variants (R312W and G302V) may only influence ATP binding and RAD51C activity due to locations in the second monomer (**Fig. 6B**). R312W removes a positively charged residue that may weaken the interaction with the negatively charged gamma phosphate group of ATP. Importantly, the R312 residue from the first RAD51C monomer was predicted to be 16 Å away from the gamma phosphate,

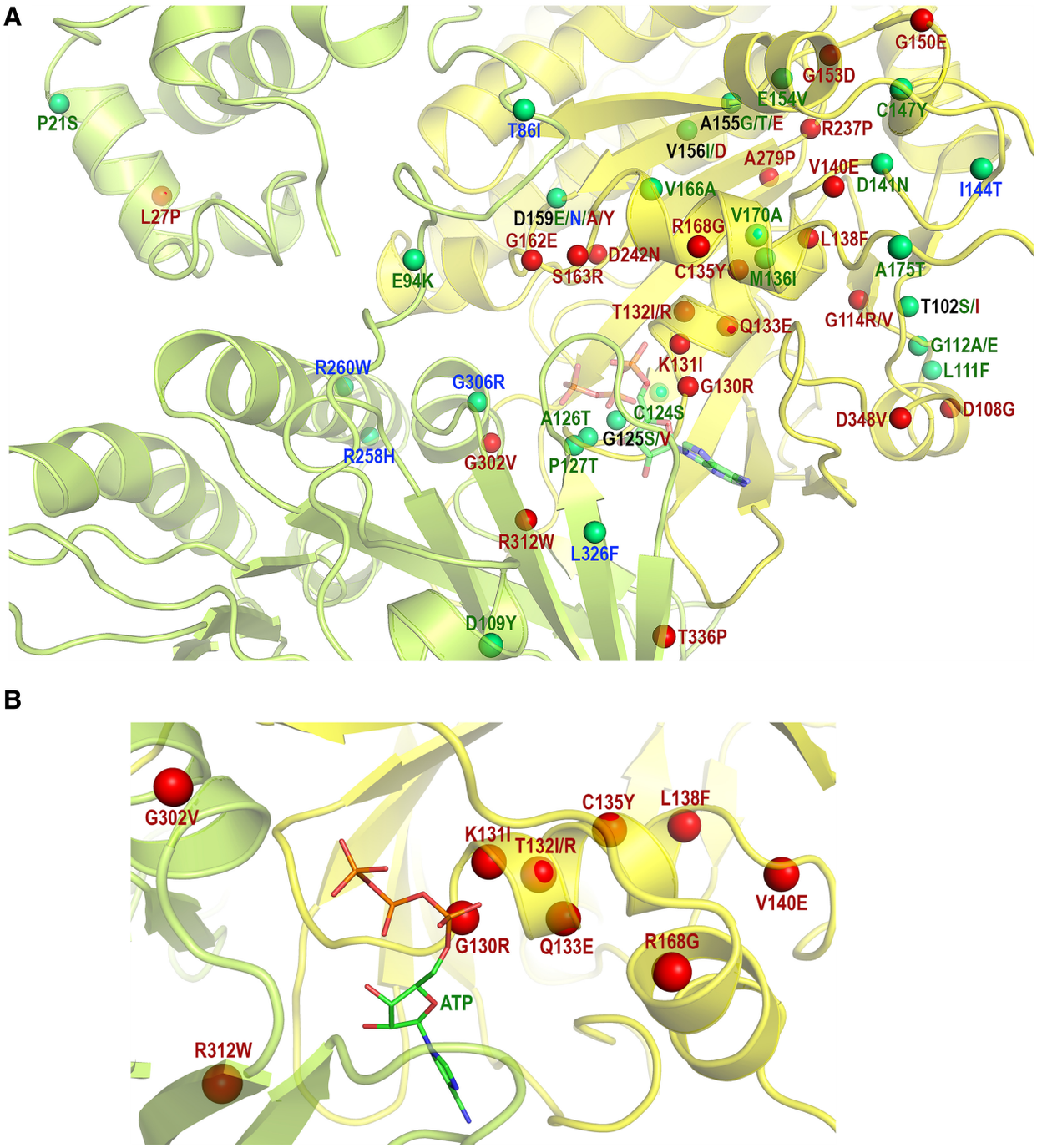

Figure 6.
Evaluation of RAD51C deleterious variants in RAD51C 3D structure prediction model. **A,** Locations of 30 neutral and 30 deleterious variants in the 3D model of two ATP-bound RAD51C monomers (yellow and green). The locations of neutral and deleterious variants are shown with green and red dots, respectively. **B,** Magnified view of the 11 deleterious variants predicted to disrupt the binding of ATP.

and not involved in ATP binding. In addition, the G302V variant disrupts a hydrophobic core and may interfere with RAD51C protomer formation. Overall, all variants that may influence interactions with ATP were found to be deleterious in the HDR and other functional assays.

In silico predictor performance based on HDR functional analysis of 173 *RAD51C* variants

The ability of the VEST4, M-CAP and REVEL sequence-based *in silico* prediction models to distinguish between deleterious and neutral variants from the HDR functional assay was assessed

Table 1. Association of functionally characterized *RAD51C* variants with breast and ovarian cancer risk.

		Overall[a]					
Phenotype	**Variant categories**	**Odds ratio (95% CI)**	***P* value**	**Case variant number**	**Case number tested**	**Control variant number**	**Control number tested**
Ovarian cancer	Deleterious	14.8 (7.71–30.36)	6.09×10^{-15}	26	17670	17	124318
	Neutral	1.32 (1.02–1.68)	0.03	73	17670	417	124318
	Truncating	7.92 (5.54–11.35)	7.06×10^{-30}	64	17670	57	124318
Breast cancer	Deleterious	3.92 (2.18–7.59)	1.45×10^{-5}	48	119531	17	124318
	Neutral	1.05 (0.92–1.21)	0.46	390	119531	417	124318
	Truncating	1.82 (1.32–2.53)	2.83×10^{-4}	101	119531	57	124318
			Non-Hispanic white				
Ovarian cancer	Deleterious	14.45 (6.12–36.09)	1.28×10^{-10}	19	12389	7	65907
	Neutral	1.26 (0.92–1.7)	0.14	54	12389	229	65907
	Truncating	8.19 (5.01–13.78)	1.96×10^{-16}	40	12389	26	65907
Breast Cancer	Deleterious	3.87 (1.7–9.05)	4.66×10^{-4}	31	75342	7	65907
	Neutral	0.92 (0.77–1.11)	0.41	242	75342	229	65907
	Truncating	1.95 (1.23–3.12)	4.24×10^{-3}	58	75342	26	65907

Note: Study excludes variants known to influence splicing and copy-number variants. Cases: breast cancer and ovarian cancer cases from women receiving germline clinical genetic testing by Ambry Genetics and GeneDx. Controls: noncancer females from the gnomAD2.1 exome and gnomAD3.1 genome reference controls and CARRIERS study population-based controls.

Abbreviation: NFE, Non-Finn European.

[a]Weighted logistic regression with control populations weighted for the relative frequency of different races and ethnicities in the cases.

(Supplementary Table S1). The optimal Matthews Correlation Coefficient RankScore threshold for REVEL (46) was 0.79 with 3 false negatives and 14 false positives. The optimal threshold for M-CAP was 0.64 with 5 false negatives and 21 false positives, whereas the optimal threshold for VEST4 was 0.67 with 4 false negatives and 22 false positives. Comparing receiver operating characteristic (ROC) curves more than 2,000 iterations using the DeLong test, the area under the curve (AUC) was significantly higher for REVEL relative to M-CAP ($P = 0.01$) and VEST4 ($P = 0.03$). The precision recall (PR)-AUC was also higher for REVEL (0.70) compared to MCAP and VEST4 (0.61 and 0.620, respectively). These results suggest that REVEL is the best of these broadly used prediction models for selecting potentially deleterious *RAD51C* variants.

RAD51C missense variants and risk of breast and ovarian cancer

To assess associations between deleterious *RAD51C* missense variants and risk of ovarian and breast cancers, the combined frequencies of deleterious variants from the HDR assay observed among ovarian ($n = 17{,}670$) and breast cancer ($n = 119{,}531$) patients qualifying for hereditary cancer clinical genetic testing by Ambry Genetics and GeneDx were compared with frequencies of deleterious variants from noncancer, female reference controls from gnomAD and the population-based CARRIERS study ($n = 124{,}318$; ref. 12). Analyses yielded significant associations with a strong risk of ovarian cancer (OR, 14.80; $P = 6.09 \times 10^{-15}$) and a moderate risk of breast cancer (OR, 3.92; $P = 1.45 \times 10^{-5}$; **Table 1**). Analyses using only gnomAD or only CARRIERS controls yielded similar results (Supplementary Tables S5 and S6). Restricting cases and controls to non-Hispanic whites and non-Finnish Europeans yielded similar associations with ovarian (OR, 14.45; $P = 1.28 \times 10^{-10}$) and breast cancer (OR, 3.87; $P = 4.66 \times 10^{-4}$; **Table 1**). Consistent with these results, *RAD51C* pathogenic PTVs were associated with high risks of ovarian cancer (OR, 7.92; $P = 7.06 \times 10^{-30}$) and increased risks of breast cancer (OR, 1.82; $P = 2.8 \times 10^{-4}$). In contrast, neutral HDR variants were not associated with clinically actionable (OR > 1.5) increased risks of either ovarian (OR, 1.32; $P = 0.03$) or breast cancer (OR, 1.05; $P = 0.46$; **Table 1**). Associations with breast cancer from the CARRIERS population-based breast cancer case–control study were attenuated, as expected for population-based rather than high risk cases (Supplementary Table S7). Overall, the HDR assay enriched for variants that were associated with increased risk of breast or ovarian cancer.

Clinical characteristics of patients with *RAD51C* deleterious missense variants

Breast cancer cases with *RAD51C* deleterious missense ($n = 46$) or PTVs ($n = 63$) from the clinical cohorts exhibited similar ages at breast cancer diagnosis of 49.4 and 50.4 years, respectively (Supplementary Table S8). Race, personal history of cancer, and breast tumor ER and HER2 status were also similar. Approximately 50% of *RAD51C* deleterious missense and PTVs were identified in patients with ER-positive breast cancer. In contrast, significantly more breast cancer cases with PTVs than deleterious missense variants had a family history of breast, ovarian, or pancreatic cancer ($P < 0.05$). Ovarian cancer cases with *RAD51C* deleterious missense ($n = 28$) and PTVs ($n = 45$) also exhibited similar ages at ovarian cancer diagnosis of 57.9 and 56.1, respectively (Supplementary Table S9).

Discussion

VUS in *RAD51C* and other cancer predisposition genes identified by germline and somatic genetic testing create challenging situations for management of patient care. Those with germline VUS in the *RAD51C* breast and ovarian cancer predisposition gene are unable to benefit from enhanced screening for breast and ovarian cancers, risk-reducing surgery for ovarian cancer, or provision of cancer risk information to family members in the same way as individuals with established pathogenic variants. Furthermore, as tumors with pathogenic variants in *RAD51C* appear to be sensitive to DNA damaging agents such as platinum and PARP inhibitors, those with germline or somatic VUS may benefit from targeted therapy in the future. Thus, uncertainties in VUS classification translate into exclusion of at-risk individuals from risk-reduction and therapeutic strategies.

Accurate clinical classification of *RAD51C* VUS and prediction of response of *RAD51C* tumors to targeted therapy, depends in large part on understanding the impact of VUS on RAD51C activity. However, functional characterization of *RAD51C* VUS for risk assessment remains elusive. Therefore, comprehensive functional analysis of 173 *RAD51C* missense variants was undertaken. Among the 173 variants, 30 were shown to reduce the HR activity of RAD51C below 25% (**Fig. 1A**). Of these, 18 were located in the small hotspot region between residues 125 and 168 containing the predicted Walker A and part of the ATP binding site. Two deleterious variants were located in the Walker B motif at residues 237 and 242, which is also predicted to contribute to ATP binding (**Fig. 1B**). All variants that were deleterious in the HDR assay had increased sensitivity to cisplatin and olaparib, a PARP inhibitor (**Figs. 1C** and **2**). In addition, 7 variants with intermediate/hypomorphic HDR activity of 25%–50% displayed intermediate drug responsiveness of 40%–80% for both cisplatin and olaparib (**Figs. 1C** and **2**). Similar effects on RAD51C activity were observed using a RAD51 foci formation assay (Supplementary Fig. S1). Thus, four functional assays using CL-V4B *Rad51c*-deficient hamster cells yielded highly consistent results for *RAD51C* variants (**Fig. 1C**).

Importantly, results in human U2OS osteosarcoma cells with stable and consistent integration of *RAD51C* cDNAs at a landing pad site showed similar results to the CL-V4B assays (**Figs. 3A** and **4**). Likewise, results from a recent study of 36 RAD51C missense variants that reported on the functional effects of reconstitution of U2OS and MCF10A RAD51C–depleted cells with full-length *RAD51C* cDNA expression constructs showed consistency with the CL-V4B results (Supplementary Table S1). While there were some differences between the results in U2OS and MCF10A cells, the CL-V4B results were always most similar to the lowest activity in either U2OS or MCF10A cells. Furthermore, all variants with HDR scores >0.5 (approximately 50% activity) in U2OS or MCF10A cells, other than the L138F-negative control, had HDR scores >1.5 (>30% activity) in CL-V4B cells, indicating consistent identification of variants with limited effects on protein function. These results overall strongly suggest that the HDR assays in CL-V4B cells reflect HDR activity in MCF10A human breast and U2OS human osteosarcoma cells.

The consistent and well calibrated results can now potentially serve as validation data for other moderate to high-throughput assays. However, while the results suggest that individuals carrying any of the 30 deleterious and the seven intermediate *RAD51C* variants in this study and the 17 deleterious variants in the 36 variant U2OS and MCF10A study may be at increased risk for both breast and ovarian cancers that may be sensitive to cisplatin and PARP inhibitors, formal classification of variants as pathogenic or benign will only be accomplished by incorporation of the well calibrated functional study results into variant classification models such as the ACMG/AMP-like model that is under development by the ClinGen affiliated Hereditary Breast Ovarian and Pancreatic Cancer (HBOP) Variant Curation Expert Panel (VCEP).

To understand the mechanism of action of the deleterious missense variants, coimmunoprecipitation experiments examining the influence of the VUS on the integrity of the CX3 and BCDX2 RAD51C complexes were performed. All 30 HDR deleterious variants from the HDR assay lost the ability to form at least one of the CX3 and BCDX2 complexes, whereas neutral variants had no effect (**Fig. 5**). In addition, intermediate/hypomorphic VUS from the HDR assay either disrupted a single RAD51C complex or dramatically reduced the levels of both complexes. Microsecond molecular dynamics simulations of the RAD51C protein revealed a core ATP-binding domain likely involved in protein complex formation (44). The presence of the deleterious variants predominantly in the core domain and the potential structural effects of these variants on the binding of ATP suggests that the conformational model may be useful for predicting the effects of VUS on ATP binding to RAD51C and to prioritize VUS for functional studies. This model also may be useful for classification of the clinical relevance of *RAD51C* variants when combined with other data in an ClinGen ACMG/AMP rule–based classification model that is currently under development by the ClinGen Hereditary Breast Ovarian and Pancreatic cancer (HBOP) Variant Curation Expert Panel (VCEP).

Pathogenic inactivating variants in *RAD51C* have been associated with increased risks of ovarian cancer (15, 16, 47–50). Most recently, a large study of families with *RAD51C* pathogenic variants estimated a high risk for ovarian cancer (RR = 7.55) and a cumulative lifetime risk to age 80 of 11%. The result from the case-control association analysis of *RAD51C* pathogenic PTVs in the current study using clinically tested ovarian cancer cases and public gnomAD reference controls yielded very similar results (OR, 7.92; 95% CI, 5.54–11.35). However, the association with ovarian cancer risk was higher for the deleterious missense variants identified in the HDR assay (OR,= 14.8; 95% CI, 7.71–30.36). Results for non-Hispanic whites only, that account for the majority of cases and controls, were very similar to those from the overall population. While the risk estimates associated with missense variants were larger than for PTVs, these differences were not significantly different. However, these results raise the possibility that deleterious missense variants may confer higher risks of ovarian cancer through dominant negative effects on RAD51C complexes. The role of *RAD51C* as a moderate risk breast cancer gene has only recently been established. While numerous small studies identified pathogenic variants in breast cancer cases, the large CARRIERS population-based case–control study showed that pathogenic variants were associated with moderate risks of ER-negative breast cancer (OR, 2.19; 95% CI, 0.97–4.49; ref. 12). Similar results were reported in the large BRIDGES study for breast cancer (OR, 1.93; 95% CI, 1.20–3.11) and ER-negative breast cancer (OR, 3.99; 95% CI, 2.20–7.26; ref. 11). In addition, a large study of family probands with *RAD51C* alterations yielded a moderate risk (RR = 1.99) with a cumulative lifetime risk of breast cancer of 11%. In this study, the deleterious HDR missense variants in *RAD51C* also were associated with moderate risk of breast cancer (OR, 3.92; 95% CI, 2.18–7.59). As with ovarian cancer, the results raise the possibility of stronger effects of missense variants than PTVs. These findings suggest that women with *RAD51C* deleterious missense variants may have cumulative lifetime risks for breast cancer between 10% and 20%. Importantly, the observation that similar proportions (approximately 40%) of deleterious missense and PTVs of *RAD51C* in this study were identified in ER-negative cases and had similar distributions of age at diagnosis (Supplementary Table S8) strongly suggests that the estimated risk of breast cancer was not caused by differences in age of diagnosis or tumor histopathology within the study population. Thus, further studies to better define cancer risks for missense *RAD51C* variants are needed.

PARP inhibitors have emerged as targeted therapy of choice for tumors deficient in homologous recombination (HR) DNA repair genes like *BRCA1/2* and several PARP inhibitors are now FDA approved for treatment of breast and ovarian cancer (51). *RAD51C*-deficient ovarian cancer patient-derived xenograft (PDX) and organoid models are known to exhibit sensitivity to PARP inhibition *in vivo* and *ex vivo*, respectively (52). All the *RAD51C* deleterious variants identified in the current study were unable to rescue the effects of both cisplatin and olaparib, further confirming the sensitivity phenotype of the *RAD51C*-deficient state. Thus, identifying pathogenic variants in *RAD51C* will likely prove important for

identification of ovarian cancer patients who may benefit from PARP inhibitors. Similarly, *RAD51C* pathogenic variants in breast tumors may confer sensitivity to PARP inhibitors. However, because not all HR-deficient tumors respond well to PARP inhibitors (53) additional functional studies of *RAD51C*-deficient ovarian and breast tumors are required to develop novel targeted therapies for these patients.

Advances in clinical testing are resulting in rapid accumulation of VUS in databases (e.g., ClinVar) that surpass the number of VUS evaluated in customized studies. However, high-throughput functional approaches to study VUS are emerging as an efficient approach to characterization of variants (54, 55). The large number of variants showing consistent results in HDR and drug response assays in the current studies will prove useful as validation standards for future high throughput approaches and will further enhance the clinical translation of *RAD51C* VUS classification into patient care.

In summary, this study provided an approach for reducing the barrier of comprehensive functional classification of *RAD51C* VUS. These results have potential implications for risk reduction and targeted therapy strategies for breast cancer and ovarian cancer for patients harboring these VUS and provide a rationale for evaluation of *RAD51C* VUS using an HDR and drug response assays and RAD51C conformational analysis.

Authors' Disclosures

G. Montalban reports grants from Fonds de recherche du Québec-Santé during the conduct of the study. L.R. Susswein is an employee of GeneDx. M.E. Roberts reports other support from GeneDx during the conduct of the study. M.L. Marshall reports other support from GeneDx outside the submitted work. S. Hiraki is an employee of GeneDx. H. LaDuca reports personal fees from Ambry Genetics during the conduct of the study and from Nest Genomics outside the submitted work. E. Chao reports other support from Ambry Genetics during the conduct of the study. T. Pesaran is an employee of Ambry Genetics. S.L. Neuhausen reports grants from National Cancer Institute during the conduct of the study. P. Kraft reports grants from National Institutes of Health during the conduct of the study. J.R. Palmer reports grants from National Institutes of Health during the conduct of the study. C.M. Vachon reports grants from NCI/NIH during the conduct of the study and from GRAIL outside the submitted work. J.N. Weitzel reports personal fees from Natera outside the submitted work. R. Karam reports other support from Ambry Genetics outside the submitted work. M.E. Richardson reports personal fees from Ambry Genetics outside the submitted work. K.S. Hruska reports other support from GeneDx, LLC during the conduct of the study. J.S. Dolinsky reports personal fees from Ambry Genetics Corporation during the conduct of the study. J. Simard reports grants from Université Laval and CHU de Quebec-Université Laval Research Center during the conduct of the study. F.J. Couch reports grants from NIH and BCRF, personal fees from AstraZeneca, nonfinancial support from Ambry Genetics, and other support from Natera during the conduct of the study. No disclosures were reported by the other authors.

Authors' Contributions

C. Hu: Data curation, formal analysis, validation, methodology, writing–original draft, writing–review and editing. **A.B. Nagaraj:** Data curation, formal analysis, validation, methodology, writing–original draft, writing–review and editing. **H. Shimelis:** Data curation, formal analysis, validation, methodology, writing–original draft, writing–review and editing. **G. Montalban:** Data curation, formal analysis, methodology, writing–review and editing. **K.Y. Lee:** Data curation, methodology, writing–review and editing. **H. Huang:** Data curation, writing–review and editing. **C.A. Lumby:** Data curation, writing–review and editing. **J. Na:** Methodology, writing–review and editing. **L.R. Susswein:** Data curation, methodology, writing–review and editing. **M.E. Roberts:** Conceptualization, resources, data curation, formal analysis, supervision, funding acquisition, validation, investigation, methodology, writing–original draft, project administration, writing–review and editing. **M.L. Marshall:** Data curation, methodology, writing–review and editing. **S. Hiraki:** Data curation, methodology, writing–review and editing. **H. LaDuca:** Data curation, methodology, writing–review and editing. **E. Chao:** Data curation, methodology, writing–review and editing. **A. Yussuf:** Data curation, methodology, writing–review and editing. **T. Pesaran:** Data curation, methodology, writing–review and editing. **S.L. Neuhausen:** Data curation, methodology, writing–review and editing. **C.A. Haiman:** Resources, data curation, writing–original draft, writing–review and editing. **P. Kraft:** Data curation, funding acquisition, investigation, methodology, writing–original draft, writing–review and editing. **S. Lindstrom:** Data curation, writing–review and editing. **J.R. Palmer:** Data curation, writing–review and editing. **L.R. Teras:** Data curation, writing–review and editing. **C.M. Vachon:** Data curation, writing–review and editing. **S. Yao:** Data curation, writing–review and editing. **I. Ong:** Data curation, writing–review and editing. **K.L. Nathanson:** Data curation, writing–review and editing. **J.N. Weitzel:** Data curation, writing–review and editing. **N. Boddicker:** Data curation, methodology, writing–review and editing. **R. Gnanaolivu:** Data curation, methodology, writing–review and editing. **E.C. Polley:** Data curation, methodology, writing–review and editing. **G. Mer:** Data curation, methodology, writing–review and editing. **G. Cui:** Writing–review and editing. **R. Karam:** Data curation, writing–review and editing. **M.E. Richardson:** Data curation, writing–review and editing. **S.M. Domchek:** Data curation, writing–review and editing. **S. Yadav:** Writing–review and editing. **K.S. Hruska:** Data curation, writing–review and editing. **J. Dolinsky:** Data curation, writing–review and editing. **S.J. Weroha:** Data curation, methodology, writing–review and editing. **S.N. Hart:** Data curation, methodology, writing–review and editing. **J. Simard:** Data curation, methodology, writing–review and editing. **J.Y. Masson:** Data curation, methodology, writing–review and editing. **Y.-P. Pang:** Data curation, investigation, methodology, writing–review and editing. **F.J. Couch:** Conceptualization, resources, data curation, formal analysis, supervision, funding acquisition, validation, investigation, methodology, writing–original draft, project administration, writing–review and editing.

Acknowledgments

This work was supported by grants from the Breast Cancer Research Foundation (to F.J. Couch); NIH [R35CA253187, R01CA225662, and P50 CA116201 Specialized Program of Research Excellence (SPORE) for breast cancer, to F.J. Couch]; the PERSPECTIVE I&I project through the Government of Canada through Genome Canada (#13529) and the Canadian Institutes of Health Research (#155865); the Ministère de l'Économie et de l'Innovation du Québec through Genome Québec; the Quebec Breast Cancer Foundation; the CHU de Quebec Foundation and the Ontario Research Fund (to J. Simard and J.Y. Masson); CIHR Foundation grant (to J.Y. Masson); Fonds de Recherche du Québec – Santé (FRQS) postdoctoral program (to G. Mer); Canada Research Chair in Oncogenetics (to J. Simard); Canada Research Chair in DNA repair and Cancer Therapeutics (to J.Y. Masson).

The publication costs of this article were defrayed in part by the payment of publication fees. Therefore, and solely to indicate this fact, this article is hereby marked "advertisement" in accordance with 18 USC section 1734.

Note

Supplementary data for this article are available at Cancer Research Online (http://cancerres.aacrjournals.org/).

Received July 21, 2022; revised October 7, 2022; accepted May 25, 2023; published first May 30, 2023.

References

1. Bianco PR, Tracy RB, Kowalczykowski SC. DNA strand exchange proteins: a biochemical and physical comparison. Front Biosci 1998;3:D570–603.
2. Kolinjivadi AM, Sannino V, De Antoni A, Zadorozhny K, Kilkenny M, Técher H, et al. Smarcal1-mediated fork reversal triggers Mre11-dependent degradation of nascent DNA in the absence of Brca2 and stable Rad51 nucleofilaments. Mol Cell 2017;67:867–81.
3. Braybrooke JP, Spink KG, Thacker J, Hickson ID. The RAD51 family member, RAD51L3, Is a DNA-stimulated ATPase that forms a complex with XRCC2*. J Biol Chem 2000;275:29100–6.
4. Liu N, Schild D, Thelen MP, Thompson LH. Involvement of Rad51C in two distinct protein complexes of Rad51 paralogs in human cells. Nucleic Acids Res 2002;30:1009–15.

5. Masson JY, Tarsounas MC, Stasiak AZ, Stasiak A, Shah R, McIlwraith MJ, et al. Identification and purification of two distinct complexes containing the five RAD51 paralogs. Genes Dev 2001;15:3296–307.
6. Rodrigue A, Lafrance M, Gauthier M-C, McDonald D, Hendzel M, West SC, et al. Interplay between human DNA repair proteins at a unique double-strand break in vivo. EMBO J 2006;25:222–31.
7. Saxena S, Somyajit K, Nagaraju G. XRCC2 regulates replication fork progression during dNTP alterations. Cell Rep 2018;25:3273–82.
8. Somyajit K, Saxena S, Babu S, Mishra A, Nagaraju G. Mammalian RAD51 paralogs protect nascent DNA at stalled forks and mediate replication restart. Nucleic Acids Res 2015;43:9835–55.
9. Sung P, Krejci L, Van Komen S, Sehorn MG. Rad51 recombinase and recombination mediators. J Biol Chem 2003;278:42729–32.
10. Takata M, Sasaki MS, Tachiiri S, Fukushima T, Sonoda E, Schild D, et al. Chromosome instability and defective recombinational repair in knockout mutants of the five Rad51 paralogs. Mol Cell Biol 2001;21:2858–66.
11. Dorling L, Carvalho S, Allen J, González-Neira A, Luccarini C, Wahlström C, et al. Breast cancer risk genes - association analysis in more than 113,000 women. N Engl J Med 2021;384:428–39.
12. Hu C, Hart SN, Gnanaolivu R, Huang H, Lee KY, Na J, et al. A population-based study of genes previously implicated in breast cancer. N Engl J Med 2021;384:440–51.
13. Loveday C, Turnbull C, Ramsay E, Hughes D, Ruark E, Frankum JR, et al. Germline mutations in RAD51D confer susceptibility to ovarian cancer. Nat Genet 2011;43:879–82.
14. Loveday C, Turnbull C, Ruark E, Xicola RMM, Ramsay E, Hughes D, et al. Germline RAD51C mutations confer susceptibility to ovarian cancer. Nat Genet 2012;44:475–6.
15. Meindl A, Hellebrand H, Wiek C, Erven V, Wappenschmidt B, Niederacher D, et al. Germline mutations in breast and ovarian cancer pedigrees establish RAD51C as a human cancer susceptibility gene. Nat Genet 2010;42:410–4.
16. Lilyquist J, LaDuca H, Polley E, Davis BT, Shimelis H, Hu C, et al. Frequency of mutations in a large series of clinically ascertained ovarian cancer cases tested on multi-gene panels compared to reference controls. Gynecol Oncol 2017;147:375–80.
17. Song H, Dicks E, Ramus SJ, Tyrer JP, Intermaggio MP, Hayward J, et al. Contribution of germline mutations in the RAD51B, RAD51C, and RAD51D genes to ovarian cancer in the population. J Clin Oncol 2015;33:2901–7.
18. LaDuca H, Polley EC, Yussuf A, Hoang L, Gutierrez S, Hart SN, et al. A clinical guide to hereditary cancer panel testing: evaluation of gene-specific cancer associations and sensitivity of genetic testing criteria in a cohort of 165,000 high-risk patients. Genet Med 2020;22:407–15.
19. Yang X, Song H, Leslie G, Engel C, Hahnen E, Auber B, et al. Ovarian and breast cancer risks associated with pathogenic variants in RAD51C and RAD51D. J Natl Cancer Inst 2020;112:1242–50.
20. Yadav S, LaDuca H, Polley EC, Hu C, Niguidula N, Shimelis H, et al. Racial and ethnic differences in multigene hereditary cancer panel test results for women with breast cancer. J Natl Cancer Inst 2021;113:1429–33.
21. Mavaddat N, Dorling L, Carvalho S, Allen J, González-Neira A, Keeman R, et al. Pathology of tumors associated with pathogenic germline variants in 9 breast cancer susceptibility genes. JAMA Oncol 2022;8:e216744.
22. Antoniou AC, Cunningham AP, Peto J, Evans DG, Lalloo F, Narod SA, et al. The BOADICEA model of genetic susceptibility to breast and ovarian cancers: updates and extensions. Br J Cancer 2008;98:1457–66.
23. Lee A, Mavaddat N, Wilcox AN, Cunningham AP, Carver T, Hartley S, et al. BOADICEA: a comprehensive breast cancer risk prediction model incorporating genetic and nongenetic risk factors. Genet Med 2019;21:1708–18.
24. Lee A, Mavaddat N, Cunningham A, Carver T, Ficorella L, Archer S, et al. Enhancing the BOADICEA cancer risk prediction model to incorporate new data on RAD51C, RAD51D, BARD1 updates to tumour pathology and cancer incidence. J Med Genet 2022;59:1206–18.
25. Lee A, Yang X, Tyrer J, Gentry-Maharaj A, Ryan A, Mavaddat N, et al. Comprehensive epithelial tubo-ovarian cancer risk prediction model incorporating genetic and epidemiological risk factors. J Med Genet 2022;59:632–43.
26. Richards S, Aziz N, Bale S, Bick D, Das S, Gastier-Foster J, et al. Standards and guidelines for the interpretation of sequence variants: a joint consensus recommendation of the american college of medical genetics and genomics and the association for molecular pathology. Genet Med 2015;17:405–24.
27. Prakash R, Rawal Y, Sullivan MR, Grundy MK, Bret H, Mihalevic MJ, et al. Homologous recombination-deficient mutation cluster in tumor suppressor RAD51C identified by comprehensive analysis of cancer variants. Proc Natl Acad Sci U S A 2022;119:e2202727119.
28. Nagaraju G, Odate S, Xie A, Scully R. Differential regulation of short-and long-tract gene conversion between sister chromatids by Rad51C. Mol Cell Biol 2006;26:8075–86.
29. Zdzienicka MZ, Simons JW. Mutagen-sensitive cell lines are obtained with a high frequency in V79 chinese hamster cells. Mutat Res 1987;178:235–44.
30. Guidugli L, Shimelis H, Masica DL, Pankratz VS, Lipton GB, Singh N, et al. Assessment of the clinical relevance of BRCA2 missense variants by functional and computational approaches. Am J Hum Genet 2018;102:233–48.
31. Matreyek KA, Starita LM, Stephany JJ, Martin B, Chiasson MA, Gray VE, et al. Multiplex assessment of protein variant abundance by massively parallel sequencing. Nat Genet 2018;50:874–82.
32. Rodrigue A, Margaillan G, Torres Gomes T, Coulombe Y, Montalban G, da Costa e Silva Carvalho S, et al. A global functional analysis of missense mutations reveals two major hotspots in the PALB2 tumor suppressor. Nucleic Acids Res 2019;47:10662–77.
33. Liu X, Wu C, Li C, Boerwinkle E. dbNSFP v3.0: A One-stop database of functional predictions and annotations for human nonsynonymous and splice-site SNVs. Hum Mutat 2016;37:235–41.
34. Waterhouse A, Bertoni M, Bienert S, Studer G, Tauriello G, Gumienny R, et al. SWISS-MODEL: homology modelling of protein structures and complexes. Nucleic Acids Res 2018;46:W296–w303.
35. Short JM, Liu Y, Chen S, Soni N, Madhusudhan MS, Shivji MK, et al. High-resolution structure of the presynaptic RAD51 filament on single-stranded DNA by electron cryo-microscopy. Nucleic Acids Res 2016;44:9017–30.
36. Pang YP. FF12MC: A revised AMBER forcefield and new protein simulation protocol. Proteins 2016;84:1490–516.
37. Richardson ME, Hu C, Lee KY, LaDuca H, Fulk K, Durda KM, et al. Strong functional data for pathogenicity or neutrality classify BRCA2 DNA-binding-domain variants of uncertain significance. Am J Hum Genet 2021;108:458–68.
38. Wiltshire T, Ducy M, Foo TK, Hu C, Lee KY, Belur Nagaraj A, et al. Functional characterization of 84 PALB2 variants of uncertain significance. Genet Med 2020;22:622–32.
39. Garcin EB, Gon S, Sullivan MR, Brunette GJ, Cian AD, Concordet J-P, et al. Differential Requirements for the RAD51 paralogs in genome repair and maintenance in human cells. PLos Genet 2019;15:e1008355.
40. Kondrashova O, Nguyen M, Shield-Artin K, Tinker AV, Teng NNH, Harrell MI, et al. Secondary somatic mutations restoring RAD51C and RAD51D associated with acquired resistance to the PARP inhibitor rucaparib in high-grade ovarian carcinoma. Cancer Discov 2017;7:984–98.
41. Min A, Im SA, Yoon YK, Song SH, Nam HJ, Hur HS, et al. RAD51C-deficient cancer cells are highly sensitive to the PARP inhibitor olaparib. Mol Cancer Ther 2013;12:865–77.
42. Chun J, Buechelmaier ES, Powell SN. Rad51 paralog complexes BCDX2 and CX3 act at different stages in the BRCA1-BRCA2-dependent homologous recombination pathway. Mol Cell Biol 2013;33:387–95.
43. Somyajit K, Subramanya S, Nagaraju G. Distinct roles of FANCO/RAD51C protein in DNA damage signaling and repair. J Biol Chem 2012;287:3366–80.
44. Lio Y-C, Mazin AV, Kowalczykowski SC, Chen DJ. Complex formation by the human Rad51B and Rad51C DNA repair proteins and their activities in vitro *. J Biol Chem 2003;278:2469–78.
45. Roy U, Kwon Y, Marie L, Symington L, Sung P, Lisby M, et al. The Rad51 paralog complex Rad55-Rad57 acts as a molecular chaperone during homologous recombination. Mol Cell 2021;81:1043–57.
46. Ioannidis NM, Rothstein JH, Pejaver V, Middha S, McDonnell SK, Baheti S, et al. REVEL: An ensemble method for predicting the pathogenicity of rare missense variants. Am J Hum Genet 2016;99:877–85.
47. Blanco A, Gutiérrez-Enríquez S, Santamariña M, Montalban G, Bonache S, Balmaña J, et al. RAD51C germline mutations found in Spanish site-specific breast cancer and breast-ovarian cancer families. Breast Cancer Res Treat 2014;147:133–43.
48. Clague J, Wilhoite G, Adamson A, Bailis A, Weitzel JN, Neuhausen SL. RAD51C germline mutations in breast and ovarian cancer cases from high-risk families. PLoS One 2011;6:e25632.
49. Thompson ER, Boyle SE, Johnson J, Ryland GL, Sawyer S, Choong DY, et al. Analysis of RAD51C germline mutations in high-risk breast and ovarian cancer families and ovarian cancer patients. Hum Mutat 2012;33:95–9.
50. Vuorela M, Pylkäs K, Hartikainen JM, Sundfeldt K, Lindblom A, von Wachenfeldt Wäppling A, et al. Further evidence for the contribution of the RAD51C

gene in hereditary breast and ovarian cancer susceptibility. Breast Cancer Res Treat 2011;130:1003–10.
51. Franzese E, Centonze S, Diana A, Carlino F, Guerrera LP, Di Napoli M, et al. PARP inhibitors in ovarian cancer. Cancer Treat Rev 2019;73:1–9.
52. Hill SJ, Decker B, Roberts EA, Horowitz NS, Muto MG, Worley MJ Jr, et al. Prediction of DNA Repair Inhibitor Response in Short-Term Patient-Derived Ovarian Cancer Organoids. Cancer Discov 2018;8:1404–21.
53. Gelmon KA, Tischkowitz M, Mackay H, Swenerton K, Robidoux A, Tonkin K, et al. Olaparib in patients with recurrent high-grade serous or poorly differentiated ovarian carcinoma or triple-negative breast cancer: a phase 2, multicentre, open-label, non-randomised study. Lancet Oncol 2011;12:852–61.
54. Findlay GM, Daza RM, Martin B, Zhang MD, Leith AP, Gasperini M, et al. Accurate classification of BRCA1 variants with saturation genome editing. Nature 2018;562:217–22.
55. Starita LM, Islam MM, Banerjee T, Adamovich AI, Gullingsrud J, Fields S, et al. A multiplex homology-directed DNA repair assay reveals the impact of more than 1,000 BRCA1 missense substitution variants on protein function. Am J Hum Genet 2018;103:498–508.